P5.1 OBSERVATION OF ATMOSPHERIC BOUNDARY LAYER AND TURBULENCE ACTIVITY OVER THE OCEAN SURFACE USING SYNTHETIC APERTURE RADAR

Pablo Clemente-Colón*
NOAA/NESDIS Office of Research and Applications, Camp Springs, Maryland

1. INTRODUCTION

Atmospheric processes can often produce identifiable signatures in satellite synthetic aperture radar (SAR) microwave backscatter images of the ocean surface (Mourad, 1999). The most common atmospheric features imaged by SAR over the oceans are in fact wind speed variability patterns ranging from simple wind fronts to well-defined mesoscale circulation features. Variations in the wind stress produce variations in sea surface roughness (Bragg waves height and distribution) and, thus, on the overall backscatter received by the radar. Any atmospheric process that produces wind speed variability at the marine atmospheric boundary layer (MABL) can potentially generate an observable SAR signature.

2. OCEAN BACKSCATTER

The dielectric constant, the surface roughness, and the local surface slope, among other factors, control the interaction of the microwave energy with the Earth's surface. Over the ocean, the high dielectric constant of water translates into high reflectivity at the microwave wavelengths. For viewing angles away from vertical incidence, a smooth ocean surface will reflect SAR energy away from the sensor. As the sea surface roughness increases, the amount of backscattered energy detected by the SAR instrument increases. Given that the roughness of an ice-free ocean surface is established by the local wind, an increase in wind speed will generally result in an increase in radar backscatter and vice versa. A decrease in the incidence or radar-viewing angle will also result in an increase of the observed radar backscatter (a SAR image is brighter on the near range side) as the radar return becomes more specular.

3. SAR-DERIVED WIND SPEED

The most common features imaged by SAR over the oceans are wind variability patterns ranging from simple wind fronts to well-defined mesoscale circulation features (Friedman et al., 2001). The response of the sea surface roughness to variations in the wind stress is being exploited in order to estimate wind speeds over the ocean from SAR observations.

A Johns Hopkins University Applied Physics Laboratory SAR wind algorithm based on the CMOD4 C-Band VV scatterometer algorithm (Stoffelen, 1997) and modified for RADARSAT-1 HH polarization was developed for NESDIS as part of the StormWatch Project (Thompson and Beal, 2000). The algorithm retrieves neutral high-resolution wind images from calibrated RADARSAT-1 SAR data using a polarization relationship between the RADARSAT-1 HH NRCS, s_o^H, and the VV NRCS obtained from CMOD4, s_o^V, given by:

$$s_o^H = \frac{\left(1+a\tan^2 q\right)^2}{\left(1+2\tan^2 q\right)^2} s_o^V\left(\mathrm{U},q,j\right), \quad (1)$$

where q is the incidence angle, U is the wind speed, j is the azimuthal viewing angle of the SAR instrument relative to the wind direction, and a is a scaling coefficient found to be 0.6 from a fit of the Unal et al. (1991) empirical data. This model assumes a polarization ratio independent of wind speed. The direction of the wind is required to properly implement the algorithm. Wind directions from forecast models, scatterometer near-coincident observations, or wind-aligned features in the SAR image itself can be used.

4. MESOSCALE CIRCULATION

Mesoscale Atmospheric Circulation systems often produce observable signatures in SAR. Because of the relatively large swath width of RADARSAT-1 ScanSAR Modes in particular (450 – 500 km), a synoptic view of the imprint of storm systems on the sea surface can often be provided. SAR is being used to observe storms in the Bering Sea and the Gulf of Alaska (Polar Lows) as well as tropical storms and hurricanes in the Western Atlantic (Clemente-Colón et al., 1999). An example of such is H. Danielle captured north of the Bahamas in the wind speed image shown in Fig. 1. In this case, the directions of the model wind vectors used agree closely with the hurricane pattern in the SAR image. In other cases, SAR can be particularly useful in providing the precise location of the storms, which can then be used to make corrections to the forecast models.

* *Corresponding author address:* Pablo Clemente-Colón, NOAA/NESDIS E/RA3, 5200 Auth Rd., Room 102, Camp Springs, MD 20746; e-mail: Pablo.Clemente-Colon@noaa.gov.

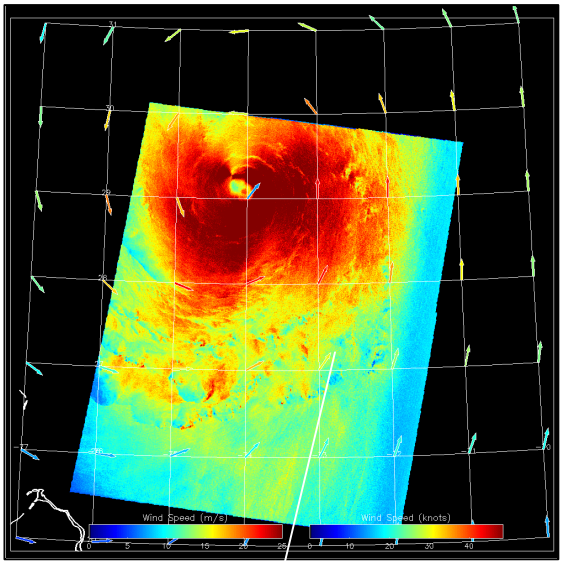

Fig. 1. H. Danielle SAR wind image on 31 AUG 98.

5. WIND ROWS AND CLOUD STREETS

Strong winds can produce clockwise and counterclockwise pairs of helices with their axis aligned in the general direction of the mean wind speed (Brown, 2000). These linear features are referred to as atmospheric roll vortices, organized large eddies (OLE), or simply wind rows. In many cases, wind rows result from cold air outbreaks from the coast or sea ice over warmer waters. Wind rows have been observed in SAR imagery and their relation to the marine boundary layer depth has been studied by a number of authors. Spacing between wind rows of 1 to over 10 km has been observed. Based on several thousands SAR images acquired over the North Pacific, Levy (2001) observed the prevalence of these features with an occurrence of over 60% in some areas.

Wind rows can be detected by visible and IR sensors from the wind alignment of associated cloud streets that develop as sufficient moisture and heat become available. Wind row cloud streets are generally aligned with the wind rather than perpendicular to the wind as is the case of cloud patterns associated with atmospheric internal gravity waves (AGWs) discussed below. Even when the general direction of the wind is not known, one can differentiate the SAR signature of wind rows from that of AGWs since at the initial stages (typically close to the coast or ice edge) wind rows tend to appear as much narrower linear features. Initially, wind rows produce bright and dark lines or streaks sharper than the smoother bright and dark wave patterns typically associated with AGWs. Once wind rows develop into cloud street-like features, they tend to look more like AGW patterns in SAR imagery. At this stage, wind rows may exhibit convective cell-like signatures that still can help differentiate them since such signatures are not typical of AGW activity.

SAR can image wind row activity even if no associated clouds patterns are present. This provides an opportunity to detect clear air turbulence conditions over the ocean. An example of this is shown in Fig. 2 where SAR backscatter has imaged wind rows as they extend offshore from the New Jersey coast. GOES IR data acquired just

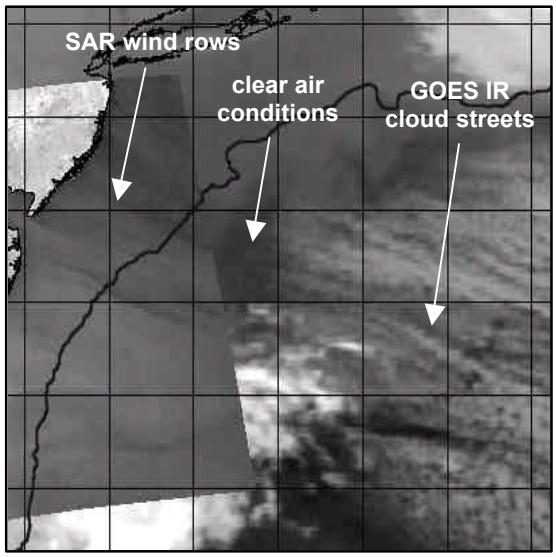

Fig. 2. SAR/GOES wind rows on 30 October 1998.

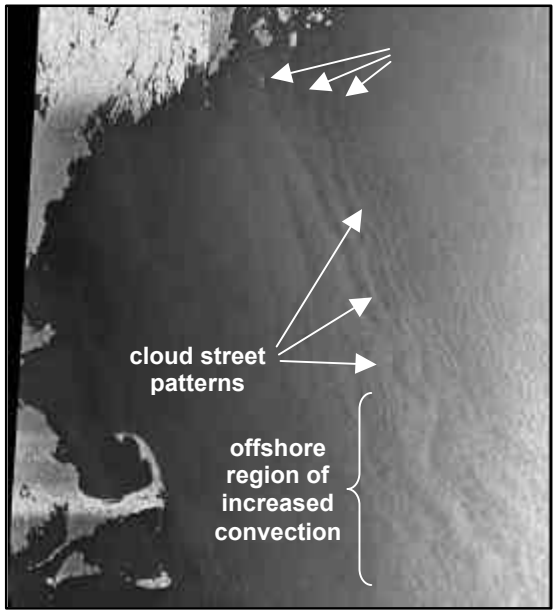

Fig. 3. SAR wind rows on 1 November 1998.

twelve minutes earlier indicate the presence of associated cloud streets 200 km away from the coast with the region where the SAR wind rows are imaged showing as cloud free. A second and perhaps more exciting example of SAR imaging of

wind rows and cloud streets is shown over the Gulf of Maine in Fig. 3. In this case, wind rows extending from the coast quickly develop into cloud street-like features. In addition to the convective cell-like patterns developed offshore, wind rows appear to exhibit meandering with respect to the wind direction. This lateral wave-like behavior of atmospheric roll vortices most surely has important implications on the stability and mean flow of the atmospheric mixed layer.

6. AGW AND VON KÁRMÁN VORTICES

As mentioned above, SAR has the ability to image the ocean surface effects of atmospheric circulation processes which produce wind speed variability at the MBL, including AGWs and vortices resulting from instabilities in the flow, even when no associated clouds patterns are present or when such patterns may be obscured by the presence of higher cloud cover. For example, AGW activity has been widely documented throughout observations of cloud patterns in visible and IR satellite imagery, where many of the patterns are interpreted as lee waves. Fig. 4 shows an impressive example of AGW activity off the Delaware coast. Several distinct AGW groups or packets with different wavelengths are imaged by SAR. AGW patterns

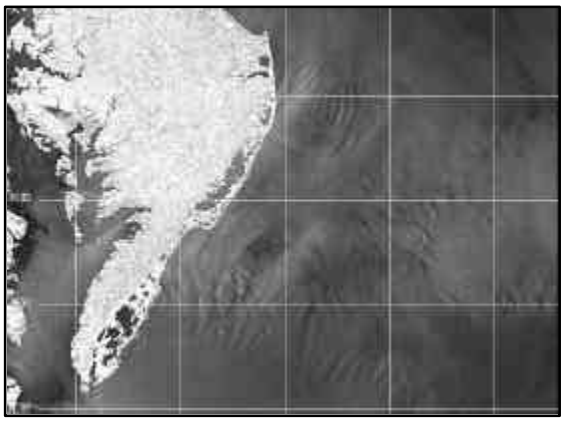

Fig. 4. SAR AGW activity on 15 January 1998.

are superimposed over one another and oriented in multiple directions. These surface conditions must be the result of complex atmospheric MBL processes at play during the time of the SAR imaging. The observed AGW wavelengths in this case range from less than 2 to over 5 km.

When air flows around a mountain or island, atmospheric vortices can also develop on the lee side under favorable conditions. These patterns consist of a double row of counter rotating vortex-pairs shedding alternately near each edge of the obstacle and can be explained by Von Kármán vortex theory. Cloud patterns associated with the wind fields produced by these vortices have also been widely documented. The SAR imprint of vortices in the Bering Sea and the Gulf of Alaska, as shown in the wind speed image in Fig. 5, are regularly observed and have been parameterized by Li et al. (2000).

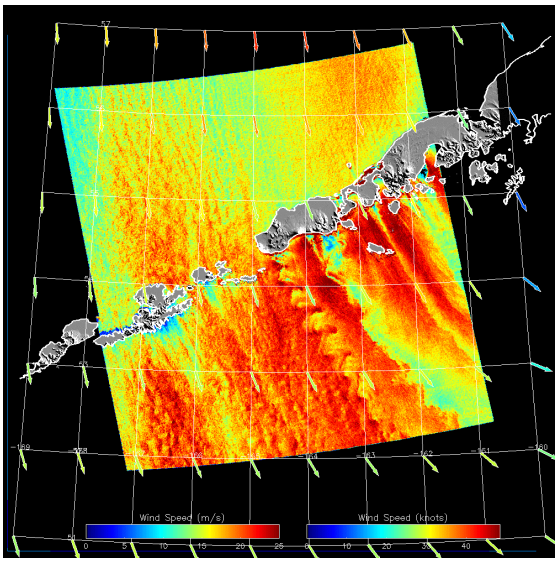

Fig. 5. SAR vortex shedding on 22 December 1999.

7. CONVECTIVE CELLS

Well-developed cell-like features imaged by SAR have been associated in previous studies with the presence of strong convective circulation (Atlas and Black, 1994; Clemente-Colón et al. 1999). These convective cells are usually characterized by having a bright side and a dark side in the SAR imagery. Melsheimer et al. (1998) attempted to explain rain cells patterns combining the volume and surface rain effects on backscatter as well as the geometry of the observation. Based on their analysis the bright side of the rain cell pattern will occur in the radar look direction, i.e., toward the near range on a convective rain cell.

A large number of observations of convective cells made as part of the AKDEMO and StormWatch projects in the Bering Sea, the Gulf of Alaska, the U.S. West and East Coasts, and the Caribbean Sea do not appear to support this conclusion. In fact, in many if not most of the cases observed, the brighter side of convective cells is not facing the radar look direction. Instead, the high/low backscatter pattern is always aligned perpendicularly to the general direction of the prevailing winds with the brighter on the leeward side. Some of the cases analyzed show the brighter side 180º from the radar look direction, for example. These observations fully support an earlier and rather simple explanation proposed by Atlas and Black (1994) in which the downdraft in the direction of the background wind adds on to produce higher backscatter on the leeward side of the cell while the downdraft opposing the

background wind decreases the total wind speed at the surface, producing relatively lower backscatter on the windward side. Under this theory, rain surface or volume effects are not required for the observed patterns to form. Thus, one can expect SAR to be able to image convective patterns that may linger even after rain activity has ceased.

An example of strong convective cell activity off Cape Cod, Maine is shown in Fig. 6. The SAR observation was made on 11 December 1998 22:32 UTC and shows identifiable individual cells off the Cape Cod region some of them as large as 40 km in diameter. Solely from the image, the direction of the prevailing winds in the region is interpreted as northeasterly, i.e., about 90º from the radar look direction (near range is on the left side of this image). The abundance of smaller convective patterns and well-defined wind rows further suggests that relatively strong wind speeds are present. The alignment of the wind rows also provide a clue as to the general orientation of the mean surface wind flow. Consistent with this assessment, wind observations recorded two minutes before the SAR pass at the Nantucket buoy indicate a wind speed of 10.8 m s^{-1} from a 329º direction. Additional wind observations made at 22:00 UTC and 23:00 UTC at the Boston buoy and the Buzzard's Bay C-Man station also confirm these wind conditions with speeds ranging from 10.5 m s^{-1} to 12.1 m s^{-1} and directions from 304º to 316º.

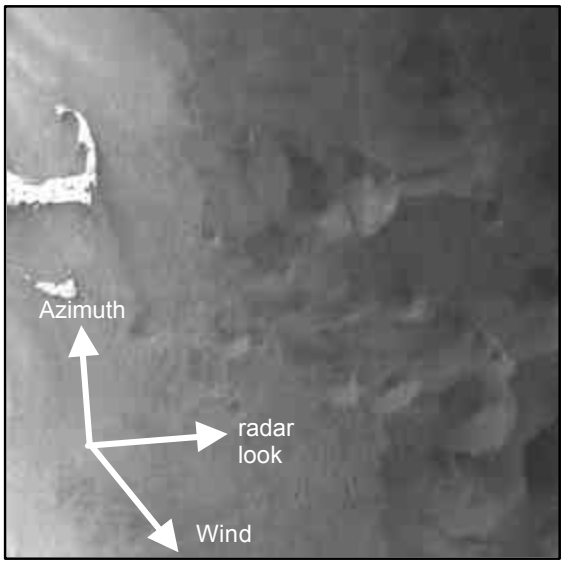

Fig. 6. SAR convective cells on 15 January 1998.

8. CONCLUSIONS

The SAR imprint of wind speed variability and of various atmospheric features over the ocean surface were presented. AGWs, wind rows and convective cells are frequently imaged by SAR and can potentially provide useful synoptic information for boundary layer and turbulence research. For example, imaging of these features when no clouds are present is suggested as a tool for detecting clear air turbulence over the ocean. When cloud patterns of these atmospheric phenomena are present, SAR imprints can still complement visible and IR observations by providing a view of conditions at the bottom of the MBL.

9. REFERENCES

Atlas D. and G. Black, 1994: The evolution of convective storms from their footprints on the sea as viewed by synthetic aperture radar from space, *Bull. Am. Meteorol. Soc.*, **75**, 1,183-1,190.

Brown, R.A., 2000: Serendipity in the use of satellite scatterometer, SAR, and other sensor data, *JHU/APL Tech. Digest*, **21(1)**, January-March, 21-26.

Clemente-Colón, P., P.C. Manousos, W.G. Pichel, and K. Friedman, 1999: Observations of Hurricane Bonnie in spaceborne synthetic aperture radar (SAR) and next generation Doppler weather radar (NEXRAD). *Proceedings EOS/SPIE Symposium on Remote Sensing Conference on Satellite Remote Sensing of Clouds and the Atmosphere IV*, 20-22 September, Florence, Italy. EUROPTO Series, **3867**, 63-70.

Friedman, K.S., T. Sikora, W.G. Pichel, and P. Clemente-Colón, 2001: Using Spaceborne Synthetic Aperture Radar to Forecast Polar Mesoscale Cyclones in the Bering Sea, *Weather and Forecasting,***16(2)**, 270-276.

Levy, G., 2001: Boundary layer roll statistics from SAR, *Geophys. Res. Letters*, **28(10)**, 1,993-1,995.

Li, X., P. Clemente-Colón, W. Pichel, and P. Vachon, 2000: Atmospheric vortex streets on a RADARSAT SAR image, *Geophys. Res. Letters*, **27(11)**, 1,655-1,658.

Melsheimer, C., W. Alpers, and M. Gade, 1998: Investigation of multifrequency/multipolarization radar signatures of rain cells over the ocean using SIR-C/X-SAR data, *J. Geophys. Res.,* **103(C9)**, 1,8867-1,8884.

Mourad, P. D., 1999: Footprints of atmospheric phenomena in synthetic aperture radar images of the ocean surface - a review. Chapter 11 in *Air-sea fluxes -physics, chemistry, and dynamics*, G. Geernaert (ed.), Kluwer Academic Publishers, Dordrecht, Holland, 640pp.Stoffelen, A. and D. Anderson, 1997: Scatterometer data interpretation: Derivation of the transfer function CMOD4, *J. Geophys. Res.*, **102(C3)**, 5,767-5,780.

Thompson, D.R. and R.C. Beal, 2000: Mapping high-resolution wind fields using synthetic aperture radar, *JHU/APL Tech. Digest*, **21(1)**, January-March, 58-67.